Research Square

Preprints are preliminary reports that have not undergone peer review.
They should not be considered conclusive, used to inform clinical practice,
or referenced by the media as validated information.

Hirudin Promotes Peripheral Nerve Repair by Enhancing Mitophagy to Suppress NLRP3 Inflammasome Activation

Rui Yan

1541275416@qq.com

Zhejiang Chinese Medical University https://orcid.org/0009-0009-5059-9019

Zhang Zhe

Wenzhou Medical College: Wenzhou Medical University

Jialuo Zhang

Wenzhou Medical College: Wenzhou Medical University

Tao Lin

Wenzhou Medical College: Wenzhou Medical University

Shanying Xiao

Wenzhou Medical University

Haotian Liu

Wenzhou Medical University

Hancheng Mao

Wenzhou Medical University

Tokai Cooper

Wenzhou Medical University

Salah Alqadhi

Wenzhou Medical University

Baolong Li

Wenzhou Medical University

Long Wu

Wenzhou Medical University

Research Article

Keywords: Angiogenesis, Hirudin, Mitophagy, Neuroinflammation, NLRP3 inflammasome, Peripheral nerve injury

Posted Date: May 25th, 2026

DOI: https://doi.org/10.21203/rs.3.rs-9582236/v1

License: This work is licensed under a Creative Commons Attribution 4.0 International License.
Read Full License

Abstract

Background: Peripheral nerve injuries cause major functional deficits and have few pharmacological options. We evaluated whether hirudin promotes peripheral nerve repair by enhancing mitophagy, preserving mitochondrial homeostasis, and restraining NLRP3 inflammasome–related pyroptosis.

Methods: Rat sciatic nerve crush injury was used to assess functional and histological recovery following systemic hirudin administration. In RSC96 Schwann cells, mitochondrial membrane potential, mitochondrial reactive oxygen species, mitophagy markers, and inflammasome activation were evaluated following a standard inflammasome activation paradigm induced by lipopolysaccharide and nigericin. The autophagy inhibitor 3-methyladenine and the selective NLRP3 inhibitor MCC950 were used to interrogate mechanistic pathways. Statistical analysis used t-tests or one-way ANOVA with Tukey's post hoc test.

Results: Network pharmacology suggested multiple enriched pathways, including the NOD-like receptor pathway, and prioritized GSDMD and interleukin-1β as candidates. In vitro, hirudin preserved mitochondrial membrane potential, reduced mitochondrial reactive oxygen species, increased mitophagy markers, and was associated with lower NLRP3/caspase-1/GSDMD activation. In vivo, hirudin improved sciatic functional index, mitigated gastrocnemius atrophy, and increased markers consistent with axonal regeneration, myelin presence, and vascular remodeling. Co-treatment with 3-methyladenine attenuated these effects, whereas MCC950 showed a similar anti-inflammatory profile.

Conclusions: These results demonstrate that hirudin promotes peripheral nerve regeneration and functional recovery largely by enhancing mitophagy, preserving mitochondrial homeostasis, and restraining NLRP3 inflammasome activation and pyroptosis. This study highlights the therapeutic potential of hirudin as a multi-target modulator in peripheral nerve injury repair. Specific pathway assignments and cellular sources are interpreted cautiously, and further validation in vivo is warranted.

Trial registration: Not applicable.

1. Background

Peripheral nerve injury (PNI) is a frequent clinical condition that often results in significant sensory and motor deficits and can, in severe instances, cause lasting disability[1]. Functional recovery following PNI is a multifaceted biological process that depends on the regenerative potential of injured axons [2]. Successful regeneration requires coordinated processes including phenotypic transformation of Schwann cells (SCs), neurovascular remodeling, and repair of neuronal cell bodies, all of which are essential for guiding axonal regrowth toward distal targets[3, 4]. After injury, SCs adopt a repair-supportive phenotype, characterized by neurotrophic factor production, secretion of inflammation-modulating cytokines, and remyelination support[5, 6].

Recent studies have identified mitochondrial dysfunction as an important contributor to impaired nerve repair. Mitochondria supply the energy required for cellular homeostasis and regulate cell death pathways[7]. Mitochondrial quality control is vital for maintaining cellular function, particularly mitophagy, the selective autophagic removal of damaged mitochondria[8]. Enhanced mitophagy facilitates the clearance of dysfunctional mitochondria, reduces mitochondrial reactive oxygen species (mtROS) levels, thereby restraining the activation of NOD-like receptor family pyrin domain-containing 3 (NLRP3) inflammasome[9].

The NLRP3 inflammasome is a macromolecular platform (NLRP3, the adapter protein ASC, and the precursor pro-caspase-1), whose activation triggers caspase-1–mediated pyroptosis and facilitates the release of pivotal pro-inflammatory cytokines such as IL-1β and IL-18. In experimental models of neurotrauma, uncontrolled NLRP3 inflammasome activation exacerbates inflammation, tissue damage, and functional loss. Hence, pharmacological strategies that enhance mitophagy while inhibiting NLRP3 activation hold promise for improving the regenerative microenvironment after PNI.

In traditional Chinese medicine, post-injury symptoms such as numbness, weakness, and pain are attributed to blood stasis and meridian obstruction, resulting in inadequate nourishment of tendons and muscles[10]. PNI was treated by activating blood circulation, and among these remedies, leeches have been used in China for approximately 2,000 years[11]. Modern pharmacological investigations have demonstrated that hirudin, as the principal bioactive constituent of leech extractions, exhibits a broad spectrum of pharmacological activities, including antitumor, antifibrotic, and wound-healing effects [12]. Hirudin has been shown to disrupt the inflammatory pathway leading to pyroptosis, and to promote vascular regeneration in settings of ischemic stroke[13]. In cardiovascular and renal injury models, hirudin facilitates the removal of damaged mitochondria, reduces mtROS, and preserves cellular homeostasis[14, 15].

Given that regulating mitochondrial dysfunction, modulating neuroinflammation, and providing vascular support are key to peripheral nerve repair, we hypothesized that hirudin could enhance Schwann cell function and axonal regeneration through mitophagy-linked restraint of NLRP3 inflammasome signaling, while also supporting vascular remodeling. This study aimed to test this hypothesis using complementary models in vivo (rat sciatic nerve crush) and in vitro (Schwann cell–based assays), to assess functional outcomes together with mitochondrial, inflammasome-related, and angiogenic readouts. By integrating these layers, our work seeks to contribute an early, pathway-level evaluation of hirudin as a multi-target modulator in PNI.

2. Methods

2.1 Drugs and Reagents

Hirudin, exhibiting chromatographic purity of ≥ 95.0% as assessed by HPLC, was purchased from MedChemExpress (HY-P2813, New Jersey, USA). MCC950 sodium (HY-12815A), LPS

(Lipopolysaccharides, HY-D1056), Nigericin (HY-127019), and 3-MA (3-methyladenine, HY-19312) were also obtained from MedChemExpress.

The following primary antibodies were acquired from HUABIO (Hangzhou, China): anti-GSDMD (1:1000, HA601046), anti-NLRP3(1:1000, ET1610-93), anti-caspase-1(1:2000, ET1608-69), anti-LC3B(1:1000, ET1701-65), anti-β-Tubulin(1:1000, EM0103), anti-S100β(1:1000, ET1610-3), anti-NF200(1:1000, ET1702-72), anti-IL-1β(1:1000, ET1701-39), and anti-ASC(1:1000, ET1611-62).

The anti-MBP primary antibody (1:1000, #AF4085) was sourced from Affinity (Jiangsu, China).

2.2 In Vitro Experiments

2.2.1 Cell Culture

RSC96 (rat Schwann cell line, CL-0199), acquired from Procell (Wuhan, China), were maintained in high-glucose DMEM (Hyclone, USA) containing 10% FBS (Gibco, USA), incubated at 37°C under 5% CO_2 atmosphere.

2.2.2 Assessment of hirudin cytotoxicity by CCK-8 (Cell Counting Kit-8) assay

Hirudin's impact on RSC96 cell viability was assessed over multiple concentrations and time points (12 and 24 h) via CCK-8 assay. Briefly, cells were plated in 96-well plates (3,000 cells/well). After treatment with hirudin (5–100 μM) or blank serum control, CCK-8 reagent (10 μL/well) was introduced and cells were incubated for an additional 2 h. Finally, absorbance readings were taken at 450 nm to determine cell viability.

2.2.3 JC-1 assay

To assess hirudin's effect on mitochondrial membrane potential (MMP, ΔΨm), evaluations were performed using RSC96 Schwann cells utilizing the JC-1 fluorescent dye, a sensitive marker for early apoptosis. RSC96 Schwann cells were plated into six-well plates and subjected to pre-treatment with LPS and Nigericin, to establish a standardized cellular response model. To simulate physiological or pathological microenvironments, conditioned medium was introduced 24 hours prior to hirudin treatment, ensuring cells were acclimated to the experimental conditions. Hirudin was then applied at specified concentrations for 24 hours to evaluate its impact on mitochondrial integrity. Following hirudin exposure, the JC-1 assay was carried out with the manufacturer's protocol (JC-1 Kit G1515-100T, Servicebio, China). Briefly, cells were cultured with JC-1 dye, which accumulates in mitochondria and exhibits a fluorescence shift from red (aggregated form in healthy mitochondria exhibiting high ΔΨm) to green (monomeric form in depolarized mitochondria displaying reduced ΔΨm). Following staining, cells were carefully rinsed to eliminate unbound dye. Fluorescence signals were acquired on a microscope fitted with dedicated filter sets: red channel (Ex/Em: 585/590 nm) and green channel (Ex/Em: 514/529 nm).

2.2.4 Mitochondrial function assessment

Mitochondrial membrane potential (MMP) and superoxide anion levels in RSC96 cells were assessed using the MitoSOX™ Red mitochondrial superoxide indicator (Beyotime, China). Following indicator staining procedure, cellular fluorescence was visualized by a fluorescence microscope (BZ-X810; Keyence, Japan).

2.2.5 Immunofluorescence (IF) staining

RSC96 Schwann cells were cultured on coverslips within 6-well plates for subsequent immunofluorescence processing. The fixation step involved 4% PFA for 10 min, followed by permeabilization in 0.1% Triton X-100 and blocking in 5% BSA (30 min each). Specimens were then treated at 4°C overnight with anti-ASC and anti-NLRP3 primary antibodies (diluted 1:200). The following day, cells were exposed to secondary antibodies (one hour at 37°C), namely Alexa Fluor 488-conjugated anti-mouse IgG and Alexa Fluor 594-conjugated anti-rabbit IgG (also at 1:200). After DAPI (1 μg/mL) was applied to label nuclei, the coverslips underwent PBS washing, were mounted on slides, and finally visualized with a Keyence BZ-X810 microscope.

2.3 In Vivo Experiments

2.3.1 Ethics Statement

The procedures for all experimental animals rigorously followed the guidelines established by the Animal Care Committee of Wenzhou Medical University, Wenzhou, China (Approval No. wydw2024-0382). All work also strictly followed the Chinese national standard (Laboratory Animal-Guideline for Ethical Review of Animal Welfare) including animal welfare, experimental protocols, and standardized housing conditions.

2.3.2 Animal grouping, modeling, and treatment

This study utilized sixty male Sprague-Dawley (SD) rats. Animals were sexually mature, specific pathogen-free (SPF), with age between six and eight weeks. Their body weight ranged from 200 to 220 grams at the beginning of the experiment. Investigators randomly assigned the rats, using a computer-generated sequence, to one of six experimental groups (n = 10 per group). The specific groups were: Control (crush injury without intervention), Sham (without crush injury), PNI□hirudin-low (crush injury treated with low dose hirudin 15mg/kg), PNI□hirudin-high (crush injury treated with high dose hirudin, 30mg/kg) [12, 15], PNI□MCC950 (crush injury treated with MCC950 at 10 mg/kg)[16], and PNI□hirudin□3-MA (Crush injury treated with a combination of high-dose hirudin and 3-MA, each at 30 mg/kg)[17].

Rats were anesthetized with an intraperitoneal injection of 2% sodium pentobarbital at a dosage of 50 mg/kg. Once a surgical plane of anesthesia was confirmed, a blunt dissection was performed on the gluteal muscles to expose the left sciatic nerve. A PNI model was generated by applying standardized compression with forceps three times. Each compression was applied for a duration of 10 seconds

approximately 5 mm distal to the sciatic notch with successive compressions separated by 10-second intervals [18], as previously described. An identical surgical procedure for sciatic nerve exposure was performed on the sham-operated rats, with the exception of nerve compression.

Rats in the crush injury groups received hirudin treatment via intraperitoneal injection, either alone or in combination with respective agonists or inhibitors. Hirudin was solubilized in physiological saline, and the final working concentration was established according to published protocols[12]. Treatment was initiated 24 hours after surgery and administered once per day. Agonists and inhibitors were administered intraperitoneally at their respective doses 30 min prior to hirudin injection each day. Both the Control and the Sham animals were administered equal volume of physiological saline.

After surgery, the muscle and skin layers were carefully sutured. All rats were then housed individually under standard conditions with easy access to food and water. Entire study was conducted in strict compliance with current guidelines for natural product pharmacology research [19].

2.3.3 Walking track analysis

To evaluate functional recovery weekly after surgery, the sciatic function index (SFI) was measured. For this assessment, rats walked along a 1-meter-long, 15-cm-wide transparent plexiglass corridor with blank white paper. Before the trial, their hind paws were pressed onto a non-toxic ink pad to coat the plantar surfaces, allowing clear footprints from both the experimental (E) and normal (N) limbs to be recorded as they moved down the track.

Three distinct parameters were quantified from each footprint: print length (PL), toe spread (TS; defined as the distance from the first to the fifth toe), and intermediary toe spread (IT; representing the span between the second and fourth toes). These measurements were substituted into the Bain's equation to calculate SFI:

$$\mathrm{SFI}=\text{-}38.3\times\frac{(\mathrm{EPL}\text{-}\mathrm{NPL})}{\mathrm{NPL}}+109.5\times\frac{\text{|}\mathrm{ETS}\text{-}\mathrm{NTS}\text{|}}{\mathrm{NTS}}+13.3\times\frac{(\mathrm{EIT}\text{-}\mathrm{NIT})}{\mathrm{NIT}}\text{-}8.8$$

where EPL, ETS, and EIT denote the experimental-side parameters, while NPL, NTS, and NIT represent the normal-side values.

SFI values typically ranges from 0 (normal function) to − 100 (complete functional impairment).[20].

2.3.4 Target muscles analysis

At the 4-week postoperative timepoint, three animals per group were randomly selected and euthanized under anesthesia induced by intraperitoneal sodium pentobarbital injection. The gastrocnemius muscles, which constitute the major muscle group in the lower limb, were carefully dissected. The wet weight ratio was calculated:

$$\mathrm{Pw}=\frac{\mathrm{W_i}}{\mathrm{W_c}}\times100\%$$

Where W_i represents the wet weight of the gastrocnemius muscle on the injured side, and W_c denotes the wet weight on the contralateral (uninjured) side. Muscle mass alterations were assessed by comparing the two values.

After 28 days of recovery, bilateral gastrocnemius muscles were dissected, fixed by immersion in 4% neutral-buffered PFA (24 h at 4°C), and subsequently prepared for histological analysis.

2.3.5 Western blot (WB) analysis

Expression of key proteins related to inflammasome activation, autophagy, and pyroptosis were assessed by WB. Tissue samples were first homogenized to extract total protein, the concentration of which was determined using a BCA protein assay kit. Subsequently, proteins were separated electrophoretically on SDS-polyacrylamide gels and electrotransferred onto PVDF membranes. Following a 1-hour block in 5% non-fat milk/TBST, the membranes were probed with relevant primary antibodies at 4°C overnight; anti-β-Tubulin served as the internal control. After thorough washing with TBST, incubations with HRP-linked secondary antibodies were carried out for 1 h at room temperature. Immunoreactive bands were finally detected using an enhanced chemiluminescence (ECL) system and analyzed quantitatively by densitometry in ImageJ, with β-Tubulin used for normalization.

2.3.6 Histological staining

After fixation and sampling as previously outlined, core segments of muscle and nerve specimens were carefully dissected, dehydrated in a graded ethanol sequence, paraffin-embedded, and sliced into 5 μm sections. Histological analysis was conducted to assess nerve regeneration and myelination status using hematoxylin and eosin (HE) and Luxol fast blue (LFB) staining.

To analyze muscle atrophy, muscle cross-sections were stained with Masson's trichrome and HE (Solarbio, Beijing, China). Collagen deposition was quantified based on collagen fiber area within three random fields per slice by Image-Pro Plus 6.0 (Media Cybernetics, USA).

2.3.7 Immunofluorescence staining

Standard immunofluorescence protocols were applied to paraffin-embedded sections of sciatic nerve tissue. The processing sequence involved fixation in 4% PFA, permeabilization using 0.2% Triton X-100, and blocking with BSA. Then sections were subjected to an incubation at 4°C overnight with target-specific primary antibodies. To assess angiogenesis at two weeks post-surgery, staining was performed using anti-CD31 and anti-α-SMA monoclonal antibodies. At the 4-week postoperative time point, anti-S100β and anti-neurofilament 200 (NF200) antibodies were used to assess myelin integrity and axonal structures, while anti-NLRP3 antibodies were utilized to investigate the mechanisms underlying peripheral nerve repair. After three-times TBST washing and treating the nerve sections with fluorophore-tagged secondary antibodies, a DAPI solution was applied for nuclear counterstaining. The stained sections were then preserved by applying an anti-fade reagent and applying a coverslip. Fluorescent images were acquired on a BZ-X810 microscope (Keyence, Japan).

2.4 Network pharmacology

The predicted targets of hirudin and PNI-related targets were analyzed and compared using the Venny online tool, with the intersection considered as putative therapeutic targets of hirudin for PNI. To explore the interactions among these targets, the intersected proteins were submitted to the STRING database, with the species parameter specified as *Homo sapiens*, to construct a protein–protein interaction (PPI) network, which was visualized and topologically assessed using Cytoscape (v3.6.1) and its Network Analyzer plugin. Hub genes were identified based on node degree. Functional enrichment analysis of these targets was conducted through Gene Ontology (GO) and Kyoto Encyclopedia of Genes and Genomes (KEGG) pathways. The top 20 enriched terms and pathways were visualized to elucidate key biological processes and signaling mechanisms.

2.5 Statistical analysis

Results are presented as mean ± SD. Statistical analyses were performed with GraphPad Prism 9.0 (GraphPad Software, San Diego, CA, USA). Two-group comparisons used two-tailed Student's t-tests; multiple-group comparisons were analyzed by one-way ANOVA followed by Tukey's post hoc test. $P < 0.05$ was considered statistically significant.

3. Results

3.1 Network pharmacology prediction of mechanism and core targets of hirudin in treating PNI

To elucidate the key constituents, therapeutic targets, and signaling mechanisms of hirudin in treating PNI, we first carried out network pharmacology analysis on hirudin. By comparing the 61 targets of hirudin with 10468 PNI-related targets and 10042 autophagy-related targets, we created a Venn diagram and discovered 17 common genes, which might be potential therapeutic targets of hirudin (Fig. 1A). Protein–protein interaction analysis suggested that Gasdermin D (GSDMD) and Interleukin-1β (IL-1β) were among the hub genes (Fig. 1B-1C). Gene Ontology (GO) enrichment analysis indicated a significant concentration of common targets within the three principal domains: biological processes, cellular components, and molecular functions (Fig. 1D). KEGG analysis revealed that 59 pathways were related to hirudin intervention in PNI, with the top-ranked pathways including the NOD-like receptor (NLR) pathway (Fig. 1E). In conclusion, these results suggest that hirudin may exert its therapeutic effects on PNI through a multi-target and multi-pathway network. The NLR pathway, as part of inflammasome-related signaling, appears to be one of the key pathways involved, with GSDMD and IL-1β potentially serving as core targets.

3.2 Hirudin suppresses NLRP3 inflammasome activation

The NLRP3 inflammasome is widely regarded as a pivotal mediator in neuroinflammation [21]. Given that hirudin possesses anti-inflammatory properties, we investigated its potential regulatory effect on NLRP3 inflammasome assembly [22].

First, viability of RSC96 cells was evaluated using CCK-8 assay following hirudin treatment at concentrations of 0, 5, 10, 25, 50, and 100 μM for 12 h and 24 h. Considering both low cytotoxicity and high pharmacological efficacy, 25 μM was selected for subsequent experiments (Fig. 2A–B).

Western blotting was subsequently conducted to assess the levels of NLRP3, ASC, cleaved and total forms of caspase-1 and IL-1β, with β-tubulin serving as the loading control. Hirudin treatment markedly decreased expression of NLRP3, ASC, cleaved caspase-1, and cleaved IL-1β in RSC96 cells relative to the LPS + Nigericin-stimulated group ($p < 0.001$; Fig. 2C–D).

Notably, ASC, like NLRP3, is an essential component for inflammasome assembly, mediating supramolecular complex formation through its pyrin domain[23]. Therefore, NLRP3 and ASC expression can serve as indicators of inflammasome activation status.

Consistently, IF staining demonstrated that hirudin markedly suppressed LPS + Nigericin-induced NLRP3 and ASC expression (Fig. 2E–F). Overall, these results indicate that hirudin attenuates NLRP3 inflammasome activation in Schwann cells under inflammatory stimulation.

3.3 Hirudin promotes mitophagy to inhibit NLRP3 inflammasome activation

Mitophagy, a critical mitochondrial quality control process, selectively removes damaged mitochondria to preserve intracellular homeostasis[8]. We therefore investigated whether hirudin modulates mitophagy during inflammasome activation.

To explore its role in hirudin-mediated regulation of the NLRP3 inflammasome, two additional groups were included by administering the autophagy inhibitor 3-MA: LPS + Nigericin + 3-MA and LPS + Nigericin + hirudin + 3-MA [24].

Using MitoTracker (mitochondrial marker) and LC3B (autophagy marker) co-staining for immunofluorescence analysis, in comparison to LPS + Nigericin group, hirudin administration markedly enhanced mitochondrial–autophagosome co-localization ($p < 0.01$), indicating a reduction in damaged mitochondria accumulation and thus enhanced mitophagy. In contrast, the 3-MA group showed decreased co-localization compared with LPS + Nigericin group ($p < 0.0001$), whereas hirudin + 3-MA group significantly reversed this hirudin-induced increase ($p < 0.01$) (Fig. 3A, 3C). These data indicate that hirudin enhances mitophagy under inflammatory conditions.

WB analysis of inflammasome-related proteins (NLRP3, β-tubulin, cleaved caspase-1, total caspase-1, cleaved IL-1β, total IL-1β, ASC) and autophagy markers (LC3B-II, LC3B-I) further supported these findings. Hirudin markedly decreased inflammasome activation markers while increasing autophagy-

related protein expression when compared to the LPS + Nigericin group. In contrast, addition of 3-MA attenuated these effects, with the hirudin + 3-MA group partially reversing this inhibition of mitophagy (Fig. 3B, 3D).

Collectively, the findings underscore that hirudin suppresses NLRP3 inflammasome activation, at least in part, by promoting mitophagy-mediated clearance of dysfunctional mitochondria.

3.4 Hirudin preserves mitochondrial homeostasis to suppress NLRP3 inflammasome activation and pyroptosis

Accumulating evidence indicates that mitochondrial damage and excessive mitochondrial ROS (mtROS) are upstream triggers of NLRP3 inflammasome activation [17]. To assess hirudin's efficacy in protecting mitochondrial homeostasis in RSC96 cells. MMP was evaluated by JC-1 and MitoTracker Green staining, while MitoSOX Red was employed to detect mitochondrial superoxide levels. The fluorescent dye JC-1 accumulates as red fluorescent J-aggregates in mitochondria with high membrane potential, but dissociates into green monomers upon depolarization. Consequently, the ratio of red-to-green fluorescence serves as a reliable indicator for quantifying the loss of mitochondrial membrane potential [25].

Compared with the LPS + Nigericin group, hirudin-treated cells exhibited a significantly higher JC-1 aggregate/monomer ratio ($p < 0.05$), approaching that of the control group, indicating preservation of MMP (Fig. 4A, 4E). Consistently, MitoSOX Red and MitoTracker Green staining revealed that hirudin markedly reduced mtROS levels and ameliorated mitochondrial depolarization ($p < 0.01$; Fig. 4B, 4F).

To further evaluate the downstream impact, live-cell imaging was performed to monitor morphological changes indicative of pyroptosis. LPS + Nigericin treatment triggered typical pyroptotic features, including plasma membrane rupture and pore formation (blue arrows), compared with normal morphology in the PBS control group (Fig. 4D). Notably, hirudin treatment reversed these abnormal morphological changes.

GSDMD is the executioner of pyroptosis, and inflammasome activation is a key upstream event controlling its cleavage from the inactive full-length form. WB analysis showed that hirudin significantly reduced NLRP3 ($p < 0.001$) and cleaved GSDMD ($p < 0.0001$) levels relative to LPS + Nigericin cells (Fig. 4C, 4G).

Collectively, these results demonstrate that hirudin preserves mitochondrial membrane potential, suppresses NLRP3 inflammasome activation, and thereby inhibits GSDMD-driven pyroptosis in RSC96 Schwann cells.

3.5 Hirudin Promotes the Recovery of Peripheral Nerve Injury

Based on its potential to alleviate neuroinflammation, we hypothesized that hirudin may facilitate the repair of PNI. To test this, the SFI, a tool for evaluating the functional status of the damaged sciatic nerve, was assessed at different time intervals after hirudin treatment. Footprints were gathered from animals across four experimental groups (Sham, PNI, PNI□hirudin-low, PNI□hirudin-high), and the SFI was computed for each corresponding set. Across all experimental cohorts, SFI values were markedly reduced in injury groups relative to Sham group at one week post-sciatic nerve crush. However, hirudin intervention significantly increased SFI values compared to the PNI cohort at each time point, which indicates that hirudin can promote functional recovery (toe extension ability) in rats (Fig. 5A – 5B, 5G). The gastrocnemius muscle, a primary target of sciatic nerve innervation in the calf, exhibited consistent alterations in the wet weight ratio (ipsilateral vs. contralateral side) (Fig. 5C – 5D, 5H). These results suggest that hirudin alleviates denervation-associated muscle atrophy after nerve injury. When the gastrocnemius loses innervation, atrophy occurs, and invasion of connective tissue follows[26]. The morphological characteristics of the target muscle tissue were assessed using Masson's trichrome staining. Histomorphometric analysis demonstrated that the collagen fiber area was markedly greater in the PNI group relative to control cohorts. Administration of hirudin effectively attenuated this fibrotic response in a manner dependent on dosage ($p < 0.0001$, Fig. 4E-F). Through the above several groups of experiments, we further verified the conjecture that hirudin promotes the recovery of peripheral nerve injury.

3.6 Hirudin promotes angiogenesis to facilitate peripheral nerve repair

Peripheral nerves possess a remarkable regenerative capacity, enabling repair even after complete transection. This process requires the collective migration of Schwann cells, which direct regenerating axons along a nascent tissue bridge to reconnect severed nerve ends. During this process, newly formed blood vessels offer structural guidance to cell movement [6, 7, 27]. Given hirudin's known angiogenic properties [12], we further investigated its effects on neovascularization during peripheral nerve regeneration.

In newly formed vessels, only CD31-positive endothelial cell staining is observed, whereas mature vessels exhibit co-localization of CD31 with α-SMA-positive smooth muscle cells. Here, immunofluorescence (IF) staining was performed to assess CD31 and α-SMA expression. The data demonstrated that hirudin therapy significantly increased both the levels of α-SMA and CD31, with a dose-dependent elevation in the density of both newly formed and mature vessels (Fig. 6A–6B), indicating an accelerated vascularization process.

To molecularly corroborate these observations, WB was employed to quantify the levels of pro-angiogenic factors HIF-1α and VEGF-A. Consistent with above results, hirudin enhanced HIF-1α and VEGF-A in a concentration-dependent manner (Fig. 6C–6D).

Overall, the data suggest that hirudin enhances angiogenesis in vivo, thereby contributing to peripheral nerve regeneration and functional recovery.

3.7 Hirudin suppresses NLRP3 inflammasome activation in Schwann cells in vivo

Based on our in vitro findings that hirudin attenuates NLRP3 inflammasome activation in RSC96 Schwann cells, we hypothesized that hirudin could exert a similar anti-inflammatory effect in vivo to promote peripheral nerve repair. To test this, we employed MCC950, a well-characterized selective NLRP3 inhibitor with potent anti-inflammatory activity, as a pharmacological comparator [28].

IF analysis of sciatic nerve sections from the Sham, PNI, PNI + hirudin, and PNI + MCC950 cohort revealed that NLRP3 level declined in the PNI + hirudin cohort compared with the PNI cohort ($p < 0.05$), while S100β expression, a Schwann cell marker indicative of regeneration, was markedly higher ($p < 0.05$). This trend aligned with the findings from the PNI + MCC950 group (Fig. 7A–B), suggesting that hirudin inhibits NLRP3 activation and facilitates Schwann cell regeneration under in vivo conditions.

Consistently, WB analysis revealed that hirudin treatment markedly reduced levels of cleaved IL-1β, cleaved caspase-1, ASC, and NLRP3 in Schwann cells of the injured sciatic nerve compared to the PNI arm—a pattern strongly aligned with observations in PNI + MCC950 arm (Fig. 7C–D).

These results indicate that hirudin, similar to the specific NLRP3 inhibitor MCC950, effectively suppresses NLRP3 inflammasome activation in vivo and promotes Schwann cell regeneration within the injured peripheral nerve.

3.8 Hirudin improves peripheral nerve repair by suppressing mitophagy-mediated NLRP3 inflammasome activation and pyroptosis

Based on the available evidence, it appears that hirudin attenuates NLRP3 inflammasome activation and pyroptosis through inhibiting mitophagy. To further confirm that hirudin's therapeutic effects on nerve repair are mediated through this suppression pathway, histological and molecular analyses were carried out on regenerated sciatic nerve segments obtained from four treatment groups.

HE staining of transverse mid-nerve sections demonstrated that axons in the Sham group were uniformly distributed, while the PNI group exhibited markedly diminished axonal density and irregular organization. In contrast, the hirudin group showed more densely packed and relatively well-aligned regenerating axons, whereas co-administration of 3-MA markedly reversed these improvements (Fig. 8A). LFB staining indicated substantially enhanced myelin formation in the hirudin group relative to the PNI group, whereas myelination was reduced in hirudin + 3-MA (Fig. 8A).

IF analysis was performed to assess regeneration of Schwann cells (S100β staining) and axons (NF200 staining). Both S100β and NF200 expression levels were markedly elevated in the hirudin group in

comparison with PNI group, whereas these increases were markedly attenuated by 3-MA co-treatment (Fig. 8B).

WB analysis of inflammasome- and pyroptosis-related proteins (NLRP3, cleaved caspase-1, total caspase-1, cleaved IL-1β, total IL-1β, ASC, cleaved GSDMD, total GSDMD) revealed that the hirudin intervention caused a robust reduction in protein levels of inflammasome activation markers and cleaved GSDMD compared to the PNI cohort. Importantly, the suppressive efficacy of hirudin on these proteins were partially reversed upon addition of 3-MA (Fig. 8C, 8D).

Collectively, these findings indicate that hirudin promotes peripheral nerve regeneration by suppressing NLRP3 inflammasome activation and pyroptosis, and these effects are dependent on modulation of mitophagy.

4. Discussion

In this research, our data prove that hirudin significantly enhanced angiogenesis in the injured nerve microenvironment, promoted nerve regeneration and functional restoration, and alleviated muscle atrophy. Mechanistically, hirudin facilitated mitophagy, thereby preserving mitochondrial homeostasis, suppressing NLRP3 inflammasome activation, and reducing pyroptosis. These findings suggest that hirudin may act as a multi-target modulator in peripheral nerve repair, extending its pharmacological profile beyond anticoagulation.

Following PNI, the ischemic and hypoxic microenvironment is a major limiting factor for nerve regeneration [29]. Angiogenesis is therefore a critical step for improving axonal regrowth and functional recovery. Newly formed blood vessels not only increase local blood flow to the injured site, thereby supplying essential energy and metabolic support, but also provide structural scaffolds for Schwann cell and axonal migration. Prior research has established that the activation of angiogenesis-associated signaling pathways, particularly those mediated by VEGF and HIF-1α, is indispensable for successful PNI repair. In this work, we observed that hirudin markedly enhanced both neovascularization and vascular maturation, accompanied by a marked elevation of HIF-1α and VEGF levels. Together, these data support the conclusion that hirudin enhances recovery after PNI by facilitating new vessel formation and mature vessel reconstruction, thereby improving local blood supply and oxygenation in the injured microenvironment.

Mitochondrial dysfunction is increasingly recognized as a central pathological mechanism after PNI, where excessive ROS production and bioenergetic collapse contribute to axonal degeneration and Schwann cell impairment. JC-1 and MitoSOX assays in our study revealed that hirudin preserved mitochondrial membrane potential and reduced mtROS levels, indicating an early protective effect on mitochondrial integrity. Moreover, the metabolic stress imposed on Schwann cells after PNI can be alleviated by improved vascularization, which enhances local oxygen and nutrient delivery and provides the energetic foundation for autophagy and mitophagy. Mechanistically, hirudin promoted mitophagy via upregulation of the AMPK/ULK1 and PINK1/Parkin pathways[12], thereby maintaining cellular energy

homeostasis and mitochondrial quality control. Efficient autophagic clearance not only removes damaged organelles and myelin debris from Schwann cells but also generates the metabolic and structural support necessary for remyelination and axonal regrowth. Our experiments confirmed that hirudin significantly increased the LC3B-II/LC3B-I ratio, indicating enhanced clearance of damaged mitochondria (Fig. 3A–3C). Importantly, the pro-mitophagy effect of hirudin was markedly attenuated by 3-MA, collectively supporting the critical role of mitophagy in hirudin-facilitated recovery from PNI.

Schwann cells are crucial for remyelination following PNI. However, pyroptosis can severely disrupt these processes. Pyroptosis is primarily triggered by NLRP3 inflammasome activation, resulting in caspase-1-mediated cleavage of GSDMD and subsequent release of large amounts of IL-1β and IL-18, thereby exacerbating cellular inflammatory microenvironment. Our findings demonstrate that hirudin significantly inhibited Schwann cell pyroptosis after PNI. In an LPS + Nigericin-induced inflammatory model, hirudin markedly lowered NLRP3, cleaved caspase-1, cleaved IL-1β, ASC, cleaved GSDMD (Fig. 2, Fig. 4, Fig. 8), indicating suppression of inflammasome activation and subsequent pyroptotic signaling. Consistently, animal experiments indicated that the effects of hirudin closely mirrored those of the selective NLRP3 inhibitor MCC950, suggesting that hirudin exerts neuroprotective effects by blocking inflammasome-mediated pyroptosis and thus improving the post-injury microenvironment. Notably, enhancing autophagy has been shown to suppress pyroptosis by facilitating ROS clearance and inhibiting NLRP3 assembly. Our results reveal that hirudin enhances mitochondrial autophagy, thereby removing damaged mitochondria and reducing mtROS accumulation. This, in turn, prevents assembly and activation of NLRP3 inflammasome, ultimately attenuating caspase-1/GSDMD-dependent Schwann cell pyroptosis.

There are still several limitations which should be noted. Firstly, this research was performed via rat model with sciatic nerve crush injury, so additional verification in large animal models as well as diverse injury models is necessary. Second, the present study relied on systemic hirudin administration, and although therapeutic effects were observed, the extent of drug delivery to the intraneural microenvironment remains uncertain. While we identified mitophagy as a key mediator, the precise signaling pathways upstream of hirudin-induced mitophagy activation remain to be elucidated. Furthermore, the long-term efficacy and optimal dosage protocol of hirudin for nerve repair require systematic evaluation, considering its anticoagulant properties.

5. Conclusion

In summary, this study establishes that hirudin promotes peripheral neural repair and functional recovery after injury primarily by enhancing mitophagy, thereby preserving mitochondrial homeostasis, suppressing NLRP3 inflammasome activation, also attenuating pyroptosis. In vivo, these effects translated into improved axonal alignment, remyelination, muscle preservation, and increased neovascularization via upregulation of HIF-1α/VEGF-A. These findings not only expand the known pharmacological profile of hirudin beyond its anticoagulant properties but also highlight mitochondrial quality control as a promising therapeutic strategy in peripheral nerve repair.

Abbreviations

3-MA, 3-methyladenine

α-SMA, Alpha-smooth muscle actin

ASC, Apoptosis-associated speck-like protein containing a CARD

CCK-8, Cell Counting Kit-8

Clv. caspase-1, Cleaved caspase-1

Clv. IL-1β, Cleaved interleukin-1β

Clv. GSDMD, Cleaved gasdermin D

GO, Gene Ontology

GSDMD, Gasdermin D

HE, Hematoxylin and eosin

HIF-1α, Hypoxia-inducible factor 1-alpha

IF, Immunofluorescence

IL-1β, Interleukin-1β

KEGG, Kyoto Encyclopedia of Genes and Genomes

LFB, Luxol fast blue

LPS, Lipopolysaccharide

MBP, Myelin basic protein

MMP, Mitochondrial membrane potential

mtROS, Mitochondrial reactive oxygen species

NF200, Neurofilament 200

NLRP3, NOD-like receptor family pyrin domain-containing 3

PPI, Protein–protein interaction

PNI, Peripheral nerve injury

S100β, S100 calcium-binding protein beta

SFI, Sciatic functional index

SC, Schwann cell

STRING, Search Tool for the Retrieval of Interacting Genes/Proteins

VEGF-A, Vascular endothelial growth factor A

WB, Western blot

Declarations

Ethics approval and consent to participate

Ethical approval for the animal experiments was granted by the Ethics Committees of the Second Affiliated Hospital of Wenzhou Medical University and Yuying Children's Hospital (wydw2024 - 0382).

Consent for publication

Not applicable

Availability of data and materials

The datasets used and/or analysed during the current study are available from the corresponding author on reasonable request.

Competing Interest

The authors unequivocally state that they possess no known competing financial interests or personal relationships that could have conceivably influenced the integrity or outcomes of the work presented in this paper.

Funding

This work was supported by the Zhejiang Province Traditional Chinese Medicine and Technology Project Management System, China (2023ZL088); the Wenzhou Major Science and Technology Innovation Project Plan, China [ZY2024009]; the Zhejiang Province Medical and Health Scientific Research Project, China (2023591475); the Wenzhou Medical University 2024 university-level scientific research project[XY2024008]; the National Natural Science Foundation of China General Project [82271421] and the Zhejiang Provincial Natural Science Foundation General Project[LY23H090009].

Authors’ contribution

RY conceived and designed the study, acquired funding, curated and formally analyzed the data, and drafted the manuscript. ZZ and JZ performed the investigations, contributed to the methodology, and drafted the manuscript. TL, HM, TC, and SA performed the investigations and contributed to the methodology. SX validated the data and created the visualizations. HL provided resources and developed the software. BL and LW critically revised the manuscript. LW also acquired funding, administered the project, and supervised the study. All authors read and approved the final manuscript.

Acknowledgements

Not applicable

References

1. K. F. Idrisova *et al.*, “Application of neurotrophic and proangiogenic factors as therapy after peripheral nervous system injury,” *Neural Regen. Res.*, vol. 17, no. 6, pp. 1240–1247, Nov. 2021, doi: 10.4103/1673-5374.327329.
2. C. Xue *et al.*, “Skin derived precursors induced Schwann cells mediated tissue engineering-aided neuroregeneration across sciatic nerve defect,” *Bioact. Mater.*, vol. 33, pp. 572–590, Dec. 2023, doi: 10.1016/j.bioactmat.2023.11.016.
3. Z. Ding *et al.*, “Role of transforming growth factor-β in peripheral nerve regeneration,” *Neural Regen. Res.*, vol. 19, no. 2, pp. 380–386, May 2023, doi: 10.4103/1673-5374.377588.
4. M. Jiang, M. Chen, and N. Liu, “Interactions between Schwann cell and extracellular matrix in peripheral nerve regeneration,” *Front. Neurol.*, vol. 15, p. 1372168, Mar. 2024, doi: 10.3389/fneur.2024.1372168.
5. T.-H. Chu and R. Midha, “Limited Myelination Capacity in Human Schwann Cells in Experimental Models in Comparison to Rodent and Porcine Schwann Cells,” *Int. J. Mol. Sci.*, vol. 26, no. 13, p. 6457, Jul. 2025, doi: 10.3390/ijms26136457.
6. E. Oshima *et al.*, “M2 macrophage-derived cathepsin S promotes peripheral nerve regeneration via fibroblast–Schwann cell-signaling relay,” *J. Neuroinflammation*, vol. 20, p. 258, Nov. 2023, doi: 10.1186/s12974-023-02943-2.
7. B. S. Mietto, P. Jhelum, K. Schulz, and S. David, “Schwann Cells Provide Iron to Axonal Mitochondria and Its Role in Nerve Regeneration,” *J. Neurosci.*, vol. 41, no. 34, pp. 7300–7313, Aug. 2021, doi: 10.1523/JNEUROSCI.0900-21.2021.
8. B. Li *et al.*, “Melatonin promotes peripheral nerve repair through Parkin-mediated mitophagy,” *Free Radic. Biol. Med.*, vol. 185, pp. 52–66, May 2022, doi: 10.1016/j.freeradbiomed.2022.04.016.
9. X. Han *et al.*, “Quercetin hinders microglial activation to alleviate neurotoxicity via the interplay between NLRP3 inflammasome and mitophagy,” *Redox Biol.*, vol. 44, p. 102010, Aug. 2021, doi: 10.1016/j.redox.2021.102010.

10. Y. Guo, Y. Ma, Y. Pan, S. Zheng, J. Wang, and G. Huang, “Jisuikang, a Chinese herbal formula, increases neurotrophic factor expression and promotes the recovery of neurological function after spinal cord injury,” *Neural Regen. Res.*, vol. 12, no. 9, pp. 1519–1528, Sep. 2017, doi: 10.4103/1673-5374.215264.
11. F.-G. Li *et al.*, “Quantitative proteomics based bioactive proteins discovery and quality control of medicinal leeches,” *J. Ethnopharmacol.*, vol. 319, p. 117117, Jan. 2024, doi: 10.1016/j.jep.2023.117117.
12. C. Junren *et al.*, “Pharmacological Activities and Mechanisms of Hirudin and Its Derivatives - A Review,” *Front. Pharmacol.*, vol. 12, p. 660757, Apr. 2021, doi: 10.3389/fphar.2021.660757.
13. W.-Q. Li *et al.*, “Hirudin alleviates acute ischemic stroke by inhibiting NLRP3 inflammasome-mediated neuroinflammation: In vivo and in vitro approaches,” *Int. Immunopharmacol.*, vol. 110, p. 108967, Sep. 2022, doi: 10.1016/j.intimp.2022.108967.
14. G. Luo *et al.*, “Hirudin inhibit the formation of NLRP3 inflammasome in cardiomyocytes via suppressing oxidative stress and activating mitophagy,” *Heliyon*, vol. 10, no. 1, p. e23077, Jan. 2024, doi: 10.1016/j.heliyon.2023.e23077.
15. Y. Xie, F. Lan, J. Zhao, and W. Shi, “Hirudin improves renal interstitial fibrosis by reducing renal tubule injury and inflammation in unilateral ureteral obstruction (UUO) mice,” *Int. Immunopharmacol.*, vol. 81, p. 106249, Apr. 2020, doi: 10.1016/j.intimp.2020.106249.
16. Y. Zhai, X. Meng, T. Ye, W. Xie, G. Sun, and X. Sun, “Inhibiting the NLRP3 Inflammasome Activation with MCC950 Ameliorates Diabetic Encephalopathy in db/db Mice,” *Mol. J. Synth. Chem. Nat. Prod. Chem.*, vol. 23, no. 3, p. 522, Feb. 2018, doi: 10.3390/molecules23030522.
17. Z. Long *et al.*, “Emodin Promotes Peripheral Nerve Repair by Modulating Inflammasome Activation Through Autophagy via the EGFR / PI3K / AKT / mTOR Pathway,” *Phytother. Res.*, vol. 39, no. 5, pp. 2324–2338, May 2025, doi: 10.1002/ptr.8469.
18. Q. Yang *et al.*, “Exosomes-loaded electroconductive nerve dressing for nerve regeneration and pain relief against diabetic peripheral nerve injury,” *Bioact. Mater.*, vol. 26, pp. 194–215, Mar. 2023, doi: 10.1016/j.bioactmat.2023.02.024.
19. X. Wang *et al.*, “Natural product pharmacology: the British Journal of Pharmacology perspective,” *Br. J. Pharmacol.*, vol. 181, no. 19, pp. 3547–3555, 2024, doi: 10.1111/bph.17300.
20. Y. H. Nam *et al.*, “Preclinical Efficacy of Peripheral Nerve Regeneration by Schwann Cell-like Cells Differentiated from Human Tonsil-Derived Mesenchymal Stem Cells in C22 Mice,” *Biomedicines*, vol. 11, no. 12, p. 3334, Dec. 2023, doi: 10.3390/biomedicines11123334.
21. Y. Li, H. Zhang, M. Liu, W. Guo, and L. Yu, “Microglia NLRP3 Inflammasomes Activation Involving Diabetic Neuroinflammation in Diabetic Mice and BV2 Cells,” *Curr. Pharm. Des.*, vol. 27, no. 24, pp. 2802–2816, Sep. 2021, doi: 10.2174/1381612827666210716104606.
22. H.-X. Yu *et al.*, “Transcriptome-Based Network Analysis Reveals Hirudin Potentiates Anti-Renal Fibrosis Efficacy in UUO Rats,” *Front. Pharmacol.*, vol. 12, p. 741801, Sep. 2021, doi: 10.3389/fphar.2021.741801.

23. J. Yuan, A. Najafov, and B. F. Py, “Roles of Caspases in Necrotic Cell Death,” *Cell*, vol. 167, no. 7, pp. 1693–1704, Dec. 2016, doi: 10.1016/j.cell.2016.11.047.
24. J. Sun *et al.*, “Berberine inhibits NLRP3 inflammasome activation and proinflammatory macrophage M1 polarization to accelerate peripheral nerve regeneration,” *Neurother. J. Am. Soc. Exp. Neurother.*, vol. 21, no. 4, p. e00347, Jul. 2024, doi: 10.1016/j.neurot.2024.e00347.
25. H. Freudenstein *et al.*, “ZEB1 stratifies the response to Sorafenib and Mdivi-1 combination therapy in hepatocellular carcinoma,” *Sci. Rep.*, vol. 15, p. 30451, Aug. 2025, doi: 10.1038/s41598-025-16379-6.
26. C. R. de S. Bueno *et al.*, “Morphofunctional Improvement of the Facial Nerve and Muscles with Repair Using Heterologous Fibrin Biopolymer and Photobiomodulation,” *Pharmaceuticals*, vol. 16, no. 5, p. 653, Apr. 2023, doi: 10.3390/ph16050653.
27. M. Bosch-Queralt, R. Fledrich, and R. M. Stassart, “Schwann cell functions in peripheral nerve development and repair,” *Neurobiol. Dis.*, vol. 176, p. 105952, Jan. 2023, doi: 10.1016/j.nbd.2022.105952.
28. H. Li *et al.*, “Therapeutic potential of MCC950, a specific inhibitor of NLRP3 inflammasome,” *Eur. J. Pharmacol.*, vol. 928, p. 175091, Aug. 2022, doi: 10.1016/j.ejphar.2022.175091.
29. R. Sandireddy, V. G. Yerra, A. Areti, P. Komirishetty, and A. Kumar, “Neuroinflammation and Oxidative Stress in Diabetic Neuropathy: Futuristic Strategies Based on These Targets,” *Int. J. Endocrinol.*, vol. 2014, p. 674987, 2014, doi: 10.1155/2014/674987.

Figures

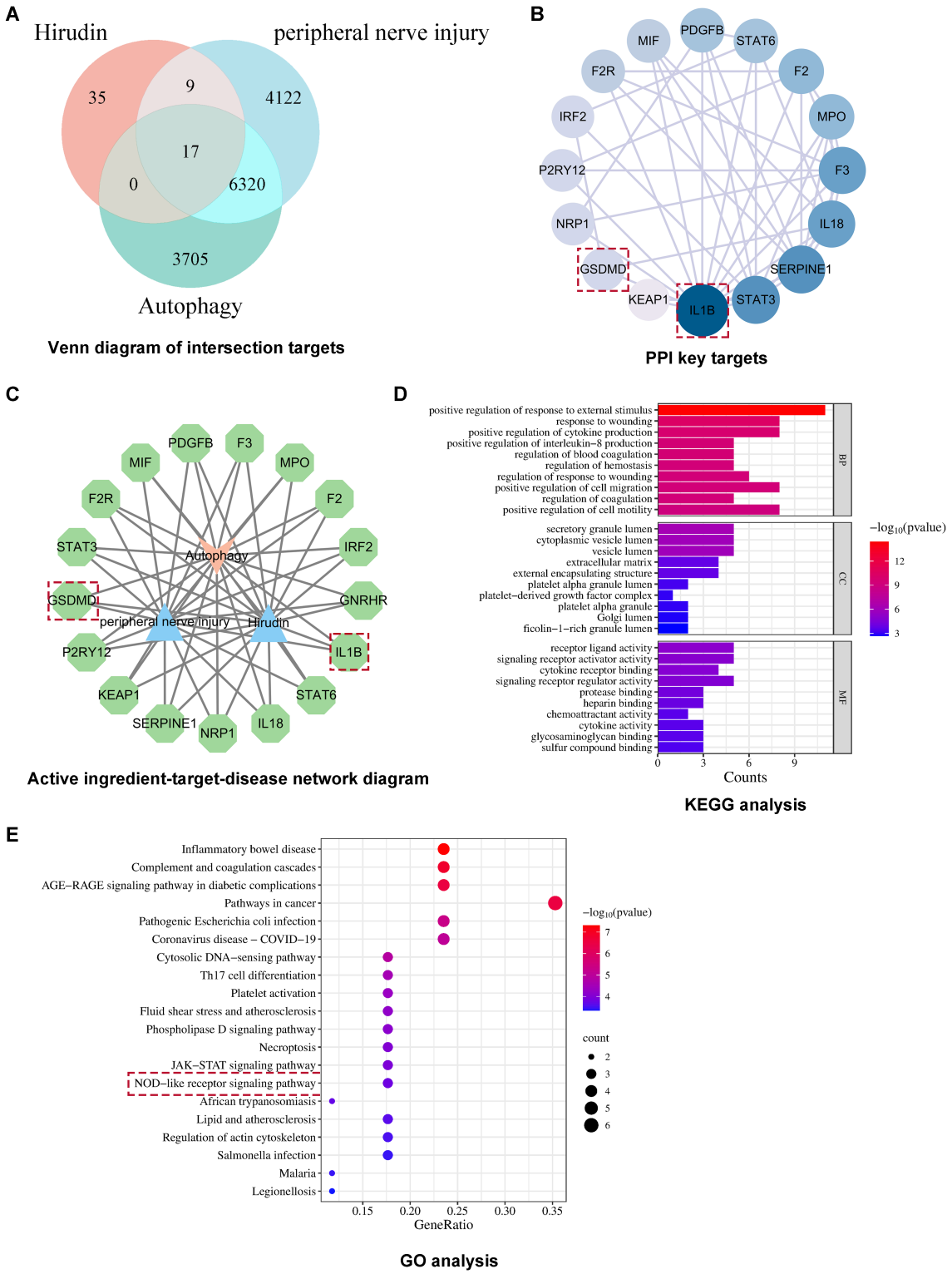


Figure 1

Network pharmacology prediction of hirudin in treating PNI. (A) Venn diagram of intersection targets among hirudin, PNI, and autophagy. (B) Protein-protein interaction (PPI) network of key targets. (C) Active ingredient-target-disease network diagram. (D) Gene Ontology (GO) analysis of common targets, categorized into Biological Process (BP), Cellular Component (CC), and Molecular Function (MF). (E)

Kyoto Encyclopedia of Genes and Genomes (KEGG) analysis of pathways related to hirudin intervention in PNI, with the NOD-like receptor signaling pathway highlighted as a key pathway.

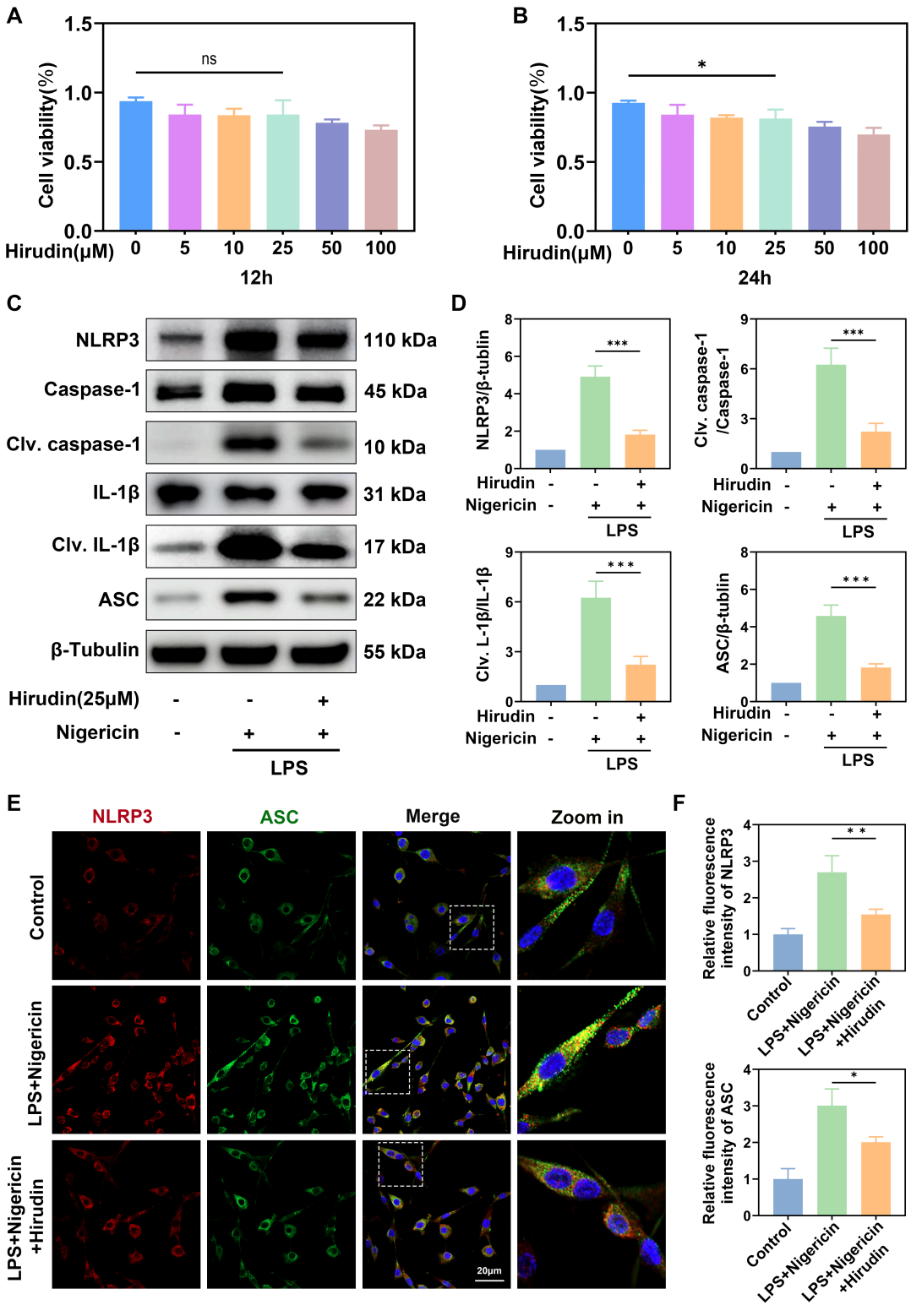


Figure 2

Hirudin attenuates NLRP3 inflammasome activation. (A-B) Cell viability of RSC96 Schwann cells treated with different concentrations of hirudin (0, 5, 10, 25, 50, and 100 μM) for 12 h and 24 h assessed by CCK-

8 assay. (C-D) WB analysis and quantification of NLRP3, β-tubulin, cleaved caspase - 1 (Clv. caspase - 1), total caspase - 1, cleaved IL - 1β (Clv. IL - 1β), total IL - 1β, and adaptor protein ASC expression in RSC96 cells. Samples were treated as indicated (hirudin: 25 μM; LPS: lipopolysaccharide; Nigericin). (E-F) Immunofluorescence staining and quantification of NLRP3 and ASC expression in RSC96 cells. Samples were treated as indicated (Control, LPS + Nigericin, LPS + Nigericin + hirudin). Nuclei were stained with DAPI (blue). Scale bar: 20 μm. Data are presented as mean ± SEM (n = 3). *$p < 0.05$, **$p < 0.01$.

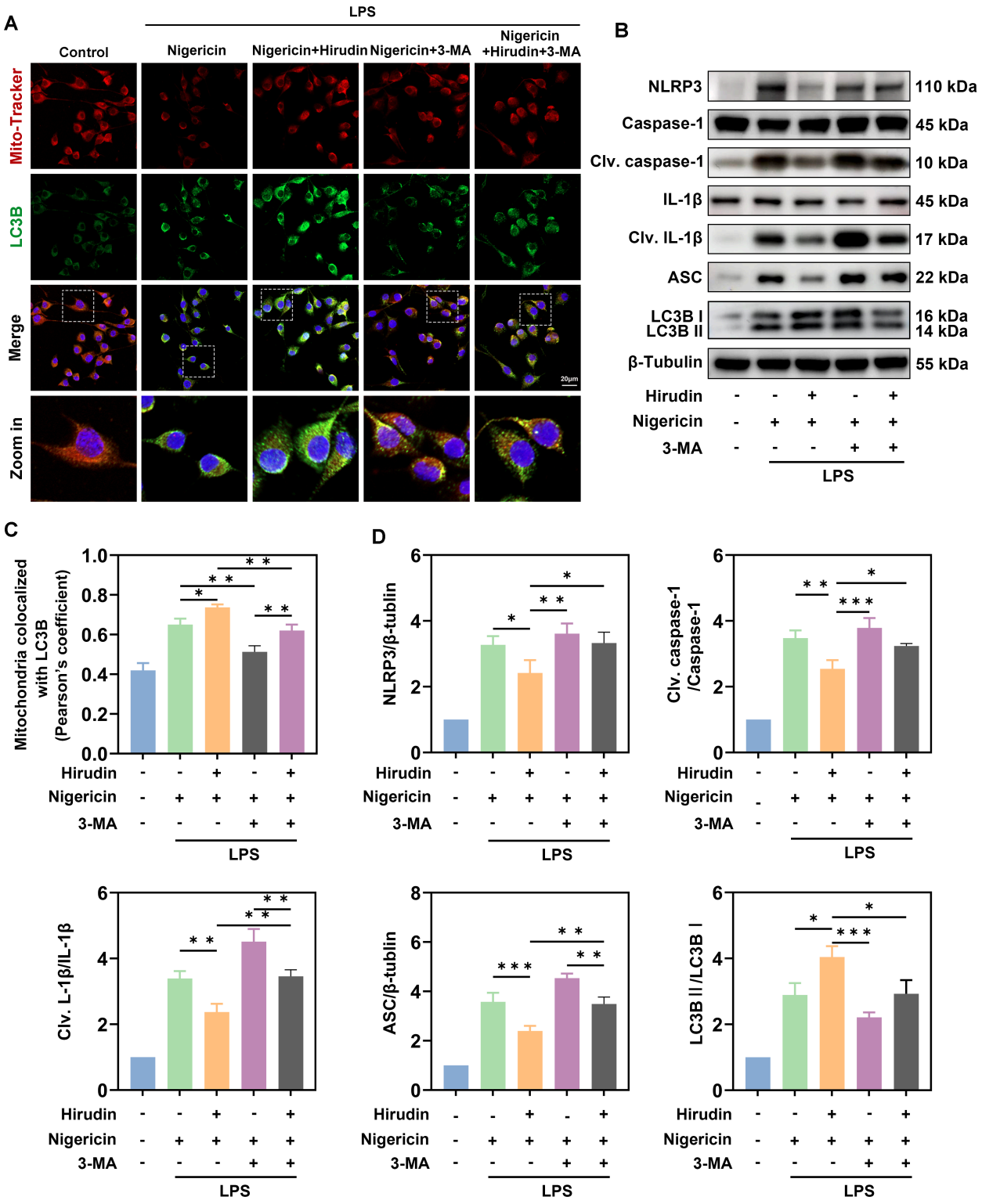


Figure 3

Hirudin promotes mitophagy to inhibit NLRP3 inflammasome activation. (A) IF staining of mitochondria (MitoTracker, red) and autophagosomes (LC3B, green) in cells treated with LPS+Nigericin. Nuclei were stained with DAPI (blue). Scale bar = 20 μm. (B) Western blot analysis of NLRP3 inflammasome components (NLRP3, caspase-1, cleaved caspase-1, IL-1β, cleaved IL-1β, ASC) and autophagy markers (LC3B-I/II). β-Tubulin served as a loading control. (C) Quantification of mitochondrial (MitoTracker) and autophagosome (LC3B) co-localization (Pearson's coefficient) from immunofluorescence images. (D) Densitometric analysis of Western blot bands normalized to β-Tubulin (for inflammasome components) or total LC3B (for LC3B-I/II). Data are mean ± SEM (n = 3). *$p < 0.05$, **$p < 0.01$, ***$p < 0.001$.

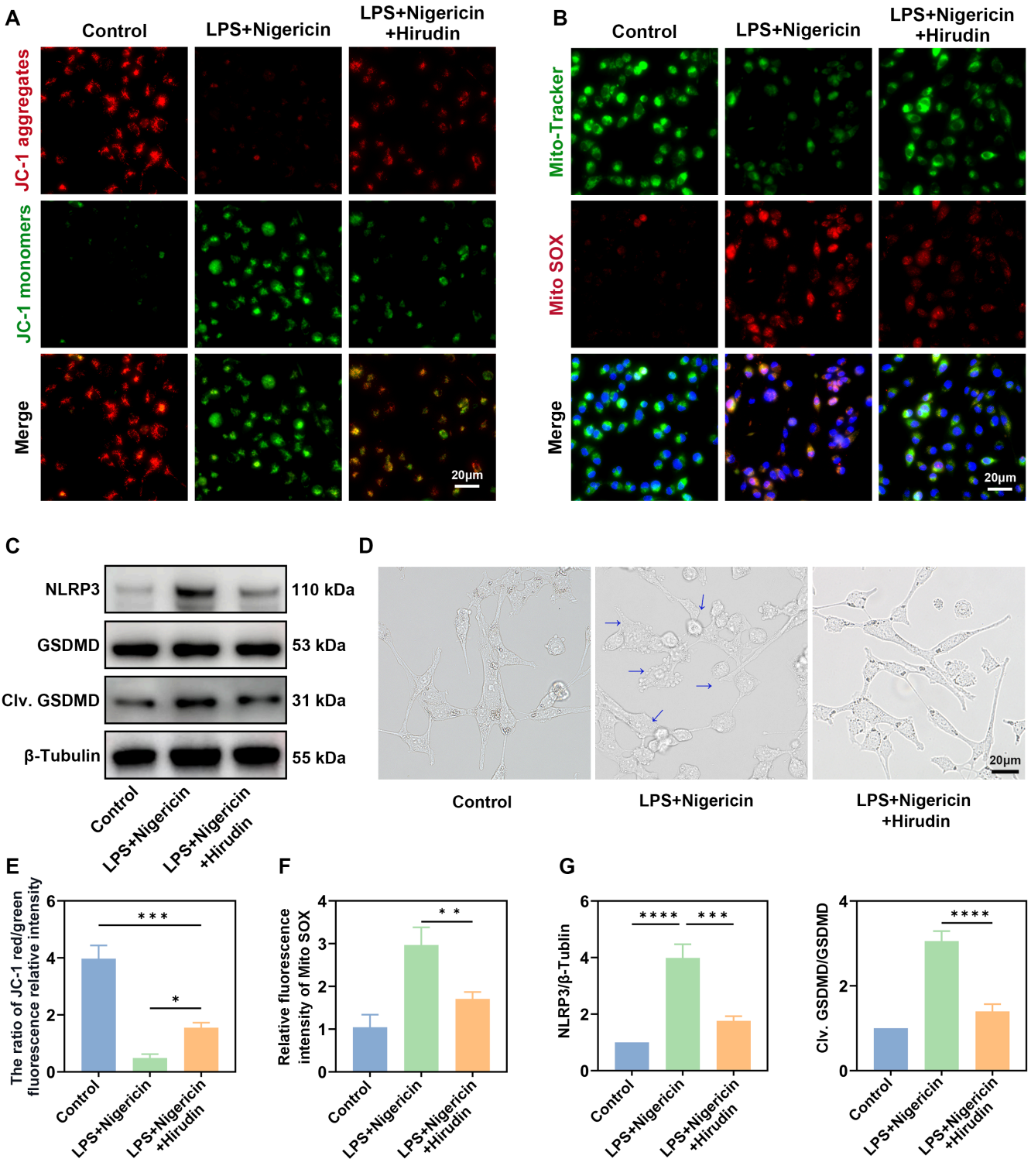


Figure 4

Hirudin preserves mitochondrial homeostasis to suppress NLRP3 inflammasome activation and pyroptosis. (A) JC-1 staining to assess mitochondrial membrane potential (MMP). JC-1 aggregates (red), JC-1 monomers (green). Scale bar = 20 μm. (B) MitoTracker (green) and MitoSOX (red) staining to visualize mitochondria and mitochondrial superoxide (mtROS) levels, respectively. Nuclei are stained with DAPI (blue). Scale bar = 20 μm. (C) Western blot analysis of NLRP3, GSDMD, cleaved GSDMD (Clv.

GSDMD), and β-Tubulin (loading control). (D) Live-cell imaging showing morphological changes indicative of pyroptosis (blue arrows). Scale bar = 20 μm. (E) Quantification of the ratio of JC-1 aggregate/monomer fluorescence intensity. (F) Quantification of relative fluorescence intensity of MitoSOX. (G) Quantification of NLRP3/β-Tubulin and Clv. GSDMD/GSDMD ratios from Western blot analysis. Data are presented as mean ± SEM (n = 3). ****p< 0.0001, ***p < 0.001.

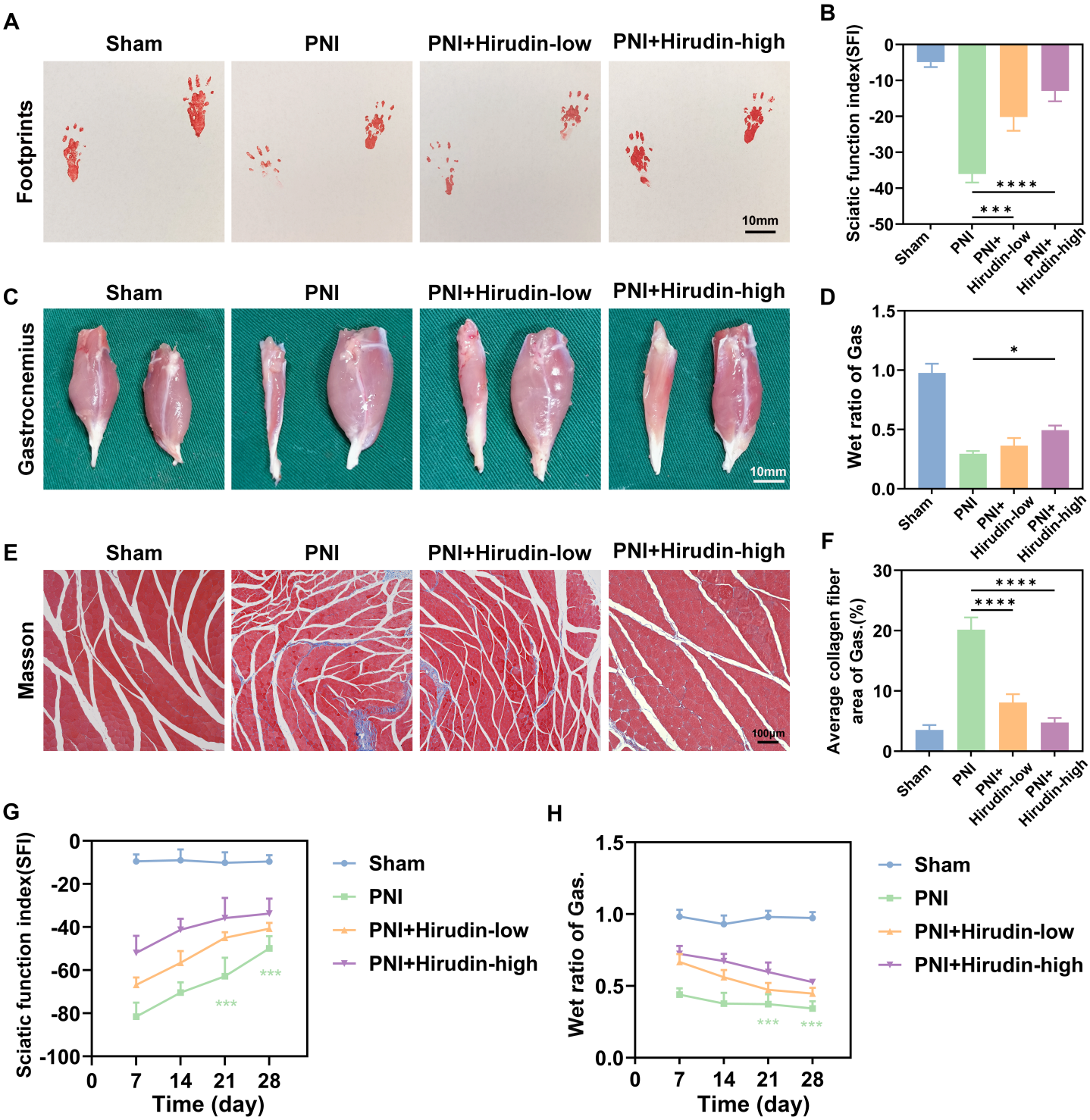


Figure 5

Hirudin Promotes the Recovery of Peripheral Nerve Injury. (A) Representative footprints of rats. (B) Sciatic functional index (SFI) values. (C) Representative gastrocnemius muscles. (D) Wet ratio of gastrocnemius. (E) Masson's trichrome staining of target muscle. (F) Average collagen fiber area. (G) Time-course of SFI. (H) Time-course of wet ratio of gastrocnemius. Data are presented as mean ± SEM (n = 3). ***$p < 0.001$, ****$p < 0.0001$.

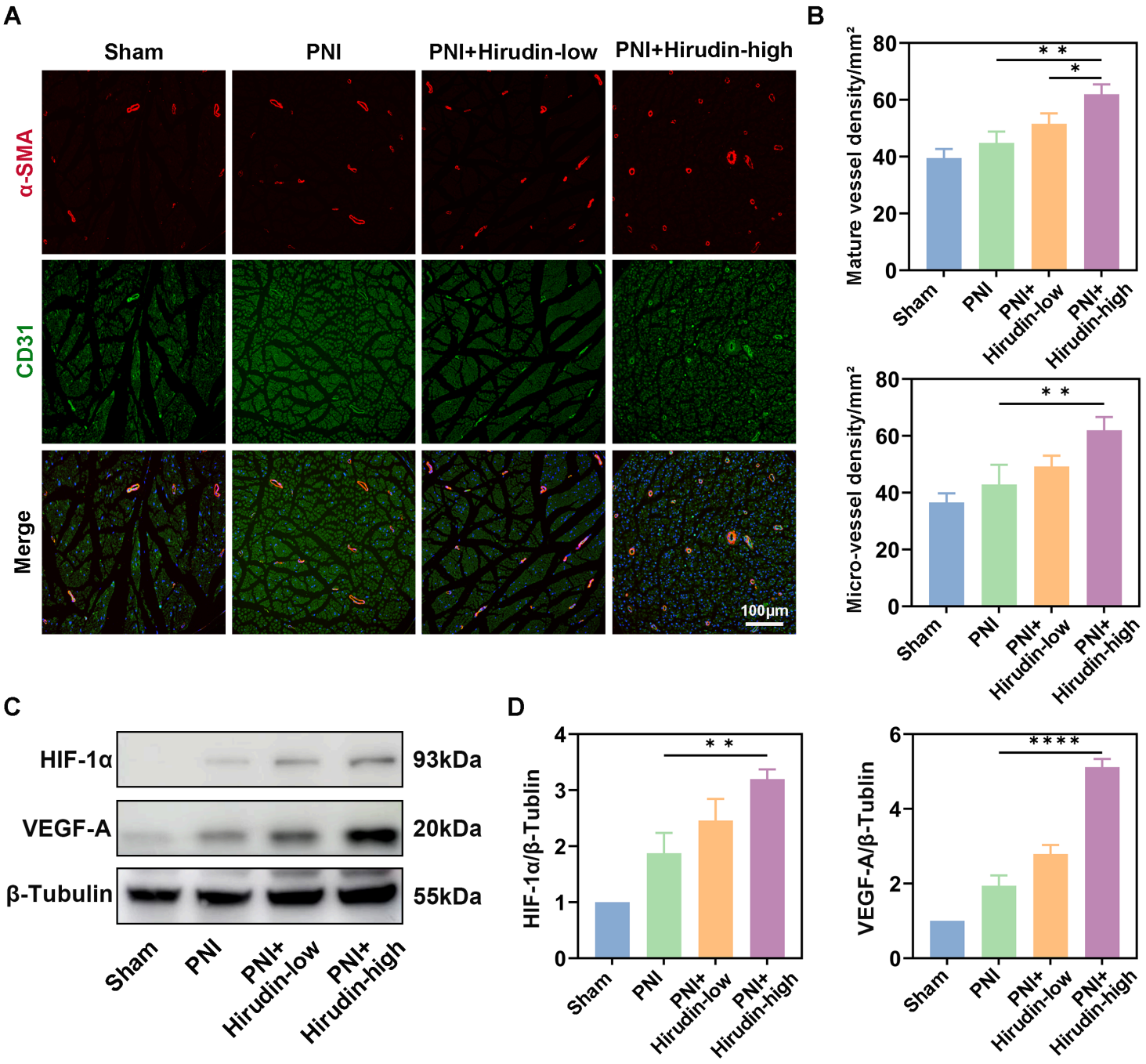


Figure 6

Hirudin promotes angiogenesis during peripheral nerve regeneration. (A) Representative immunofluorescence (IF) images showing α-SMA (red), CD31 (green). Scale bar = 100 μm. (B)

Quantification of mature vessel density and micro-vessel density in each group. (C) Western blot analysis of HIF-1α, VEGF-A, and β-Tubulin (loading control) expression in nerve tissue from each group. (D) Quantification of HIF-1α/β-Tubulin and VEGF-A/β-Tubulin ratios from Western blot results. Data are presented as mean ± SEM (n = 3). *$p < 0.05$, **$p < 0.01$, ****$p < 0.0001$.

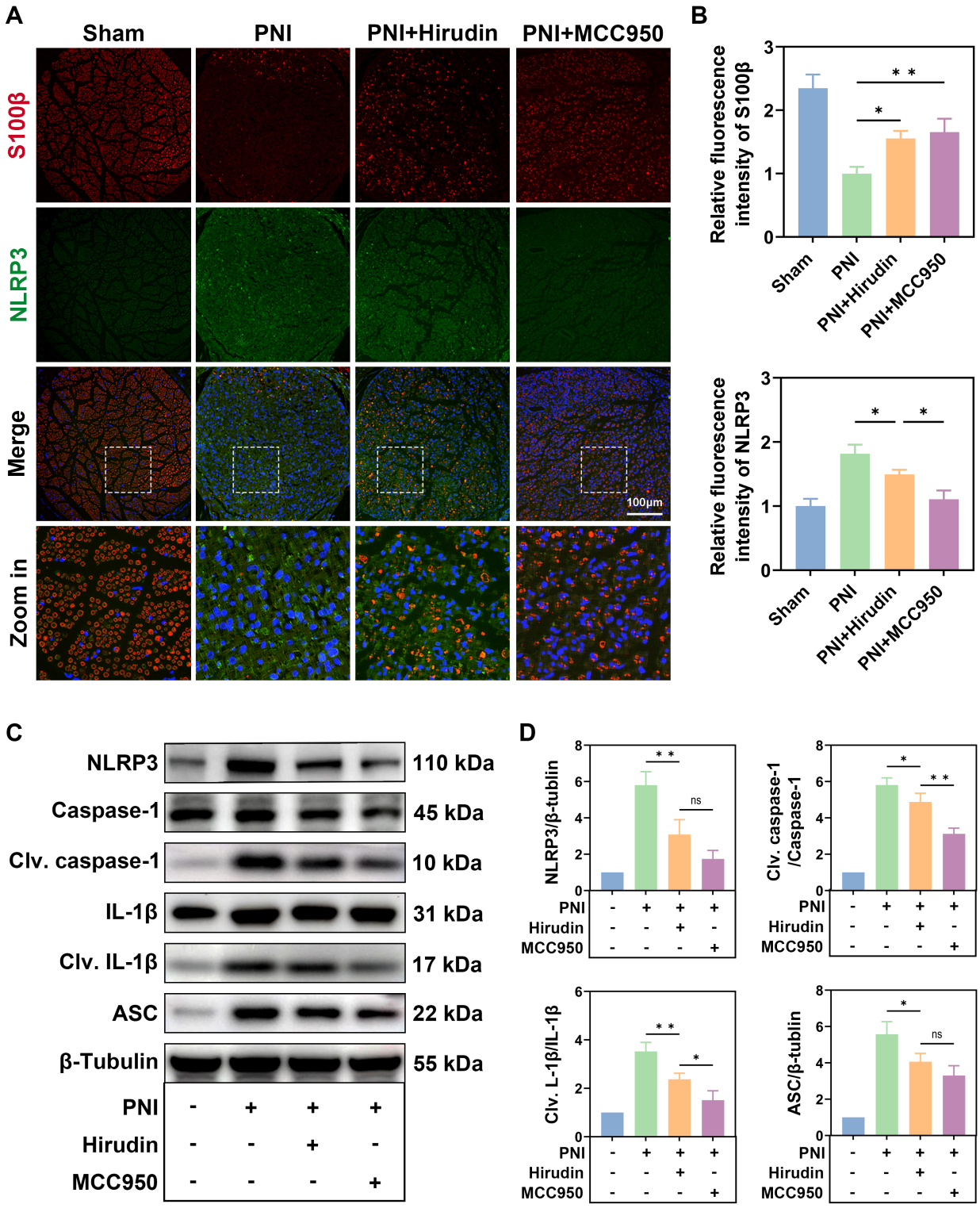


Figure 7

Hirudin suppresses NLRP3 inflammasome activation in Schwann cells *in vivo*. (A) Immunofluorescence staining of S100β (red, Schwann cell marker) and NLRP3 (green) in sciatic nerve sections. Nuclei were stained with DAPI (blue). Scale bar = 100 μm. (B) Quantification of relative fluorescence intensity of S100β and NLRP3. (C) Western blot analysis of NLRP3, caspase-1, cleaved caspase-1 (Clv. caspase-1), IL-1β, cleaved IL-1β (Clv. IL-1β), ASC, and β-Tubulin in sciatic nerve lysates. (D) Quantification of Western blot results. Data are presented as mean ± SEM (n = 3). *$p < 0.05$, **$p < 0.01$, ns: not significant.

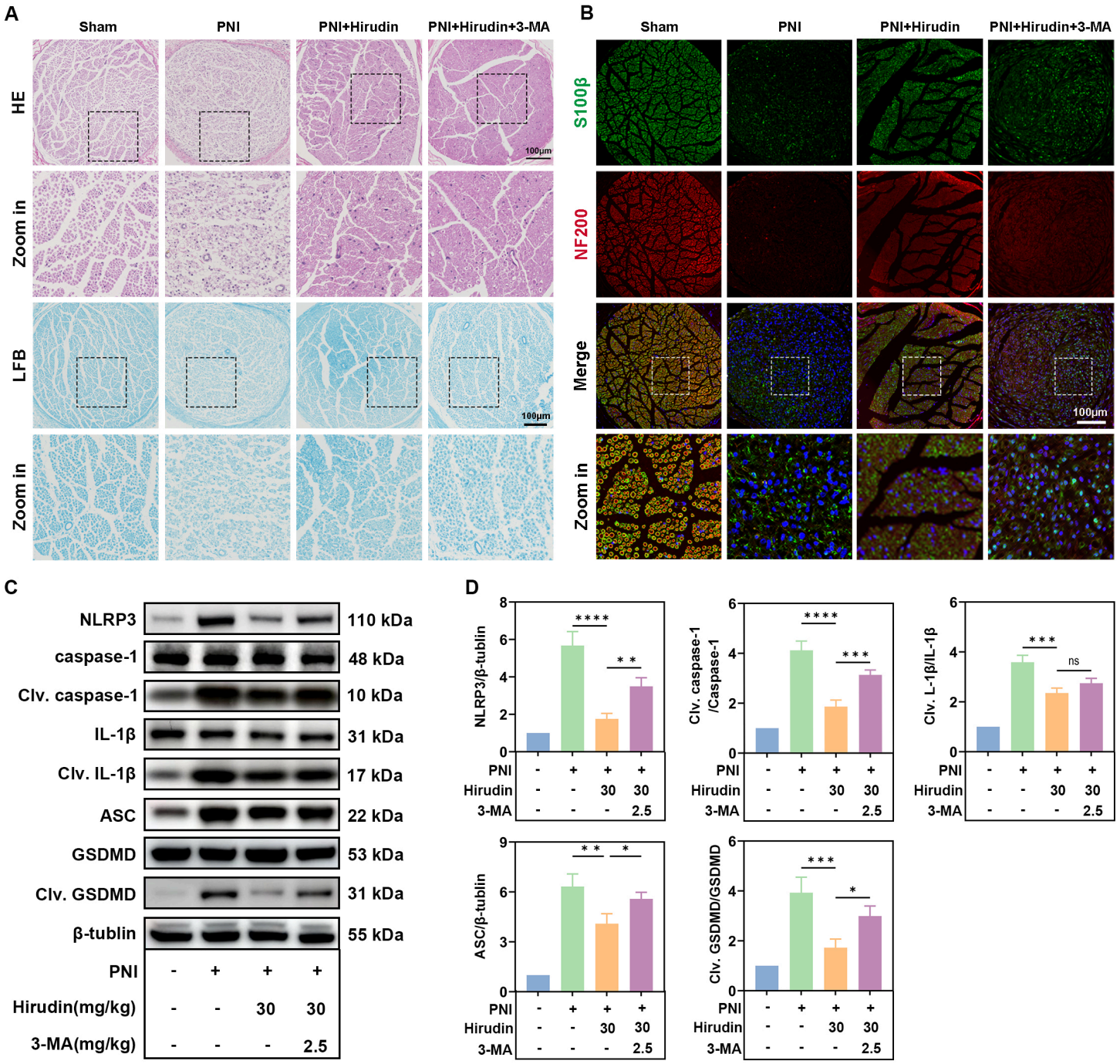


Figure 8

Hirudin improves peripheral nerve repair by suppressing mitophagy-mediated NLRP3 inflammasome activation and pyroptosis. (A) Hematoxylin–eosin (HE) and Luxol fast blue (LFB) staining. Scale bar =100 μm. (B) Immunofluorescence (IF) analysis of Schwann cell (S100β, green) and axon (NF200, red) regeneration. Nuclei were labeled with DAPI (blue). Scale bar = 100 μm. (C) Western blot analysis of NLRP3 inflammasome- and pyroptosis-related proteins (NLRP3, caspase-1, cleaved caspase-1 (Clv. caspase-1), IL-1β, cleaved IL-1β (Clv. IL-1β), ASC, GSDMD, cleaved GSDMD (Clv. GSDMD)). β-tubulin was used as a loading control. (D) Statistical analyses of the Western blot results. Data are presented as mean ± SEM (n = 3). *$p < 0.05$, **$p < 0.01$, ***$p < 0.001$, ****$p < 0.0001$.

Supplementary Files

This is a list of supplementary files associated with this preprint. Click to download.

- graphicalabstract.png
- wbforfig2.jpg
- wbforfig3.jpg
- wbforfig4.jpg
- wbforfig6.jpg
- wbforfig7.jpg
- wbforfig8.jpg